This new technique promises to become a powerful tool not only for hyperfine spectroscopy but also for γ-optical experiments. The standard experiment in the future will be the time-resolved observation of forward scattering from a polycrystalline target instead of the pure nuclear reflection from a single crystal which has been used to date. Using the time of excitation, which is known precisely and the spectrum of the delayed resonant quanta from the sample, the hyperfine interaction parameters may be determined within a few hours, even with resonant counting rates of only 1 Hz [2.34].
The use of synchrotron radiation may allow the Mössbauer effect to be observed in new isotopes. Such isotopes would need low-energy excited nuclear levels but need not have appropriate parent nuclei and hence they are not given in Table 1.1.
Additionally, this technique may be especially promising for magnetic field and EFG structure studies in crystals [2.35], and the measurement of the total external reflection of sub-μeV beams of high brilliance may be useful in the analysis of near surface layers (see subcec. 2.5 and 3.8).

2.4. Angular Dependences of the Scattered γ -radiation

The angular dependence of intensities is also important in conventional Mössbauer spectroscopy despite the fact that these dependences are not so sharp as in diffraction. It is of special importance in studies of surface layer where the Mössbauer spectra are the superposition of several partial spectra. For example, if $E_M^m(E_Q^m) >> \Gamma_{nat}$ for each of the partial spectra then, since line intensities corresponding to the transition between different sublevels possess different angular dependences, spectra recorded at the scattering angles where these differences are maximized, are easier to interpret.
In another limiting case when $E_M^m(E_Q^m) \sim \Gamma_{nat}$, it is practically only the analysis of the angular dependence of the resonantly scattered radiation that permits the origin of line broadening in the Mössbauer spectrum to be understood.
Let us find what determines the intensity dependence on the scattering angle in the absence of interference. Suppose that a nucleus gives its excitation energy by a cascade of γ-quanta. The emission of a γ-quantum, followed by a change of the total nuclear momentum by L > 1, results in a definite orientation of the nuclear spin with respect to the direction of the emitted γ-spectrum. Let us assume that the emission of the subsequent γ-quantum occurs immediately after the emission of the preceding one. Radiation from such an oriented nucleus will be anisotropic. If the nuclear orientation is changed by perturba-

tions, the angular distribution of the subsequent γ-quanta will be also changed. The angular distribution of the direction of two successive γ-quanta is independent of whether the two quanta have been emitted or whether resonant scattering has occurred. This has made it possible to use the well developed theory of angular correlations [2.35] in resonant scattering of γ-quanta. In this theory, the directional correlation function W(θ) of resonantly scattered γ-quanta with respect to the direction of the primary beam should be the same as for the two successively emitted γ-quanta in transitions between levels with the same parameters as for the levels corresponding to resonant scattering. There are theoretical expression for the correlation functions W(θ) for all cases of interest [2.37,38]. It should be noted that Mössbauer scattering allows the observation only of the integral time dependence of the angular correlation function, since it is impossible to determine the exact moment of absorption of the incident γ-quantum.

The correlation function W(θ) is determined by the directional distribution of radiation for every γ-transition and by the Clebsh-Gordon coefficients. If the excited nucleus is not affected by any fields changing its orientation, the angular distribution of the γ-quanta for a given transition with respect to a chosen quantization axis is given by

$$F_L(\theta) \sim \sum_{m_e, m_g} P(m_e)\, G(m_e, m_g)\, F_L^M(\theta) \quad , \qquad (2.49)$$

where $P(m_e)$ are relative populations of all sublevels m, $F_L^M(\theta)$ is the angular function of γ-rays for the transition between sublevels ($M = m_e - m_g$). Functions $F_L^M(\theta)$ depend only on the radiation multipolarity. For M1 transitions $F_L(\theta)$ is a sum of three terms with the angular dependences

$$F_1^0(\theta) = 3 \sin^2 \theta = 2 - 2P_2(\cos \theta) ,$$

$$F_1^{\pm 1}(\theta) = 3(1 + \cos^2 \theta) / 2 = 2 + P_2(\cos \theta) .$$

If the excited nuclei are randomly oriented, i.e. all the $P(m_e)$ are equal in any coordinate system, it follows from (2.49) that $F_L(\theta)$ is independent of θ and that radiation is isotropically emitted.

Generally, the directional correlation function is determined by the angular function for both the absorption process $(F_L^M(\theta))_a$ and the scattering process $(F_L^M(\theta))_s$. However, it is convenient to choose the direction of the quantization axis to coincide with the direction of the first quantum emitted in a cascade, since the function W(θ) is determined only by the function $(F_L(\theta))$.

For given transition multipolarity the directional correlation function is usually written in the form

$$W(\theta) = 1 + A_{22}P_2(\cos\theta) + ... + A_{k_m k_m}P_{k_m}(\cos\theta)\,. \qquad (2.50)$$

k_m is given by the selection rule $k_m = \min(2I_e, 2L)$. The coefficients A_{kk} can be explicitly calculated since they can be represented by two factors of the same form, each one being determined by the properties of one of the transitions in a cascade. If there are hyperfine fields, either static or fluctuating, a perturbation of angular correlations occurs. In a semiclassical approach, interactions of the nuclear magnetic dipole moment with the magnetic field H_{eff} , or the nuclear electric quadrupole moment with the electric field gradient EFG, result in the appearance of a rotation moment and the nucleus begins to precess about the symmetry axis (the quantization axis). Such changes in the nucleus orientation lead to a change in angular correlations. Coefficients A_{kk} in (2.50) are to be multiplied with the perturbation factors $G_{kk}(t)$, which are, in general, time dependent and depend also on the nature and energy of hyperfine interactions. Expression (2.50) now takes the form

$$W(\theta,t) = \sum_k A_{kk}G_{kk}(t)\,P_k(\cos\theta) \quad .$$

In this approach the random perturbation will not change the shape of the angular correlation function but will only diminish the coefficient at $P_k(\cos\theta)$.

The most important feature of the integrated perturbation factors for a randomly oriented static interaction (i.e. a scatterer of an ideal polycrystallite) is that they have finite lower limits G_{kk}. If the quantization axis is randomly oriented, the integrated angular correlation will not disappear even for very strong static hyperfine interactions in the solid. For axially symmetric fields :

$$G_{kk} = 1 / (2k + 1)$$

For M1 transition $G_{kk} = G_2 = 0.2$.

In a single crystal scatterer the angular distribution is completely determined by the crystal orientation with respect to the scattered radiation. If the direction of H_{eff} or EFG coincides with the direction of the incident radiation, then the relative populations $P(m_e)$ characterizing the nuclei orientation in the scatterer remain constant. At any energy of hyperfine interactions the correlations will be unperturbed. In other cases of static interactions the correlations are perturbed.

For time-dependent hyperfine interactions the angular correlations may vanish completely. Such a situation in the Mössbauer effect for ^{57}Fe is realized in paramagnetic substances. Indeed, the direction of H_{eff} changes stochastically at each nucleus. There are no quantization axes, whose populations could remain constant, hence all the sublevels are equally populated irrespective of the chosen quantization axes. Hence the directional correlation becomes isotropic. Therefore, the Mössbauer γ-quanta resonantly scattered from a scatterer whose Mössbauer spectrum is a single line of width Γ_{nat} will have an isotropic distribution.

Returning to the static hyperfine interactions let us now consider resonant scattering of the magnetic dipole radiation when the overlap of the spectrum components may be neglected. The angular distribution $W_1(\theta)$ of the components' intensities of the quadrupole doublet for the ($\pm 1/2 \Leftrightarrow \pm 3/2$) transition, and $W_2(\theta)$ for the ($\pm 1/2 \Leftrightarrow \pm 1/2$) transition, may be written as

$$W_1(\theta) = \frac{1}{16}(25 - 15\cos^2\beta_1 - 15\cos^2\beta_2 + 9\cos^2\beta_1\cos^2\beta_2) ,$$

$$W_2(\theta) = \frac{9}{16}(1 + \cos^2\beta_1 + \cos^2\beta_2 + \cos^2\beta_1\cos^2\beta_2) , \qquad (2.51)$$

where θ is the angle between vectors k_0 and k_f, angles β_1 and β_2 specify the orientation of k_0 and k_f with respect to the quantization axis.

If the scatterer is an ideal polycrystallite the experimentally observed angular dependence (2.51) is to be averages over all orientations of the EFG tenzor to give

$$W_1(\theta) = W_2(\theta) = 1 + 0.05\, P_2(\cos\theta) . \qquad (2.52)$$

This means that even when the quadrupole interaction energy is very high, the angular correlations do not vanish completely. If $E_Q^m \approx \Gamma_{nat}$, i.e. on scattering of the γ-quantum with a given energy, the excited state of the scattering nucleus is not known, and the perturbation factor is written [2.39] as:

$$G_2 = 0.2\,[1 + 4 / (1 + E_Q/\Gamma^2)] . \qquad (2.53)$$

When $\Gamma_{nat} \leq 2\Gamma_{nat}$, the angular distribution of the resonantly scattered radiation will determined by the nature of line broadening. For example, if the broadening is due to the difference in the isomer shifts caused by nonequivalent positions of the resonant atoms then the angular distribution of the intensity of the scattered radiation will be isotropic. If the broadening is due to small quadrupole splitting the angular distribution is

$$W(\theta) = 1 + 0.25\, G_2\, P_2(\cos\theta)\,, \qquad (2.54)$$

where G_2 is given by (2.53), and the anisotropy of the radiation intensity may be large. When the quadrupole interaction energy increases expression (2.54) in the limiting case transforms into (2.52).

The anisotropy of the resonantly scattered radiation also depends on the anisotropy of the factor f' . At $E_Q^m < \Gamma$ the factor f' has little effect on the angular dependence. Increasing E_Q requires that the anisotropy of the f' factor be taken into account. Now (2.52) may not be obtained from (2.51) as before since angular dependences of the Mössbauer effect probability in the scatterer should be introduced into the angular dependences of the resonantly scattered radiation (2.51) before averaging. The angular dependences of the scattered radiation intensity are strongly affected by the factor f' anisotropy. This provides an efficient method of experimentally investigating the factor f'.

If the scatterer is an ideal polycrystalline antiferromagnet, where the effective magnetic fields are strong and randomly oriented, the dependence of the intensities on the scattering angle for the first and the sixth lines of the spectra - $W_1(\theta)$, for the second and the fifth lines - $W_2(\theta)$, and for the third and the fourth lines $W_3(\theta)$, are given by the following expressions [2.11,37] :

$$W_1(\theta) = \left(\frac{3}{8}\right)^2 \frac{26 + 2\cos^2\theta}{15}\,,$$

$$W_2(\theta) = \frac{1}{8} \quad \frac{19 + 3\cos^2\theta}{15}\,, \qquad (2.55)$$

$$W_3(\theta) = \left(\frac{1}{8}\right)^2 \frac{82 - 6\cos^2\theta}{15}\,.$$

To obtain the spectral line intensities, expressions (2.55) have to be averaged over θ, and for a thin sample the intensity ratios will be 3 : 2 : 1 : 1 : 2 : 3 .

2.5. Mössbauer γ-quanta Scattering as a Method of Surface Study

Let us analyse the line shape of scattering Mössbauer spectra when γ-quanta are detected, and the energy distributions of the resonant quanta. Similar problems for transmission have been considered in Sect. 2.1. Experiments in geometry (Fig. 2.9) are used in a variety of studies, e.g. diffraction, angular correlations, phase analysis. In studies of angular dependences this geometry allows the best angular resolution to be achieved when using large scatterers. We start the analysis with the spectra obtained in this geometry.

Let us make some simplifying assumptions. At first, let there be no splitting of the energy levels in either the source or the absorber. The recoilless part of the source γ-radiation of integral intensity I_0 may be written as

$$I_M(E,S) = \frac{2f}{\pi\Gamma} I_0 L(E,S) \ . \qquad (2.56)$$

For this part of the beam it is always necessary to take into account the dependence of the interaction probability on the energy parameters E and S. Unless otherwise stated, the total beam I_0 is normalized to unity. If the energy distribution of the γ-quanta is of prime interest, the normalized beam $J_M(E,S)$ is called the energy distribution of the γ-quanta. This can be used to evaluate the spectral shape and the intensities of the detected radiation which can be obtained by integrating over all the γ-quanta energies. The beam or the intensity of radiation will be denoted by I(S).

The shape of the energy distribution of radiation changes as it penetrates the scatterer. At a certain depth x it is given by

$$J_M(E,S,x) = \frac{2f}{\pi\Gamma} L(E,S) \exp\left[-\mu_a(E)x \csc\gamma_1\right] , \qquad (2.57)$$

$$\mu_a(E) = \mu_r(E) + \mu_a \ , \quad \mu_r(E) = \sigma_0 f' n_a \frac{(\Gamma_a/2)^2 W(\theta)}{(E - E_a)^2 + (\Gamma_a/2)^2} , \qquad (2.58)$$

where $\theta = \gamma_1 + \gamma_2$.

If the energy distribution of the Mössbauer radiation at a depth x is known together with the differential cross sections for all the scattering processes contributing to the detected intensity and the thickness and composition of the scatterer, then the line shape of the Mössbauer spectrum and the energy distribution of the scattered radiation can be found. Both components of the recoilless and non-recoilless resonantly scattered radiation have different energy distributions. Resonant self-absorption of the scattered radiation in the sample may cause the partial contributions of the two components to the resulting Mössbauer spectrum to be quite different from the ratio f'/(1 - f').

Let us consider first the resonant scattering process without the loss of recoil energy and find the energy distribution $J_r(E',S,x)$ for γ-quanta scattered by a layer $dx/\sin\tilde{a}_1$ at a depth x in the scatterer

$$\frac{dJ_r(E',S,x)}{dx / \sin \gamma_1} = n_a \int_{-\infty}^{\infty} J_M(E,S,x) \frac{d^2\sigma}{dE\, dE'} dE , \qquad (2.59)$$

where n_a is the number of resonant nuclei per unit volume.

For the general case the process cross section in (2.59) is a function of both the incident γ-quanta energy and the energy E' of the γ-quanta emitted as a result of scattering. For an isotropic crystal in the absence of diffraction effects the differential cross section of the process can be written in the form [2.40,41] :

$$\frac{d^3\sigma}{d\omega\, dE\, dE'} = \frac{\gamma}{2\pi} \frac{\Gamma_a^2}{4} \frac{\sigma_0}{1+\alpha} f'^2 W(\theta) \frac{1}{[(E'-E)^2 + \gamma^2/4]\,[(E'-E_0)^2 + \Gamma_a^2/4]} , \qquad (2.60)$$

where the function $W(\theta)$ is normalized to 4π , and γ is the ground state width due to the radiation field. The width γ is very small and by appropriate modification of (2.60) may be taken as zero. This is usually done in the following way. As the incident radiation is generally not monochromatic, we can assume it to have a Lorentzian distribution of width Γ. To describe the scattering of this radiation, γ in (2.60) can be replaced by Γ. If the centre of gravity of the energy distribution of the incident radiation L(E,v) is shifted relative to the resonance energy in the scatterer (say, by $5\Gamma_{nat}/2$, as in Fig.2.10a), there will be two lines present in the scattering spectrum at energies E and E_0.

The total differential resonant scattering cross section without recoil energy loss, when the energy distribution L(E,v) of the incident radiation is taken into account, is obtained by integration of (2.60) over the energy of scattered γ-quanta

$$\frac{d^2\sigma}{d\omega\, dE} = \frac{\sigma_0}{1+\alpha} \frac{\Gamma_a(\Gamma_a+\Gamma)}{4} \frac{f' W(\theta)}{(E-E_a)^2 + [(\Gamma+\Gamma_a)/2]^2} . \qquad (2.61)$$

In order to obtain the energy distribution of γ-quanta scattered recoillessly by a layer dx at a parameter S, (2.57) and (2.60) can be substituted in (2.59):

$$\frac{dJ_r(E',S,x)}{dx \,/\, \sin\gamma_1} = \frac{\sigma_0 f'^2 f\, \Gamma\, \Gamma_a^2\, n_a}{8\pi(1+\alpha)}$$

$$\frac{\exp[-\mu_a(E')x\,\csc\gamma_1]\, d\omega}{[(E'-E_s-S)^2+\Gamma^2/4]\,[(E'-E_a)^2+\Gamma_a^2/4]}\, W(\theta)\,, \qquad (2.62)$$

where dω is the solid angle within which the source radiation reaches the scatterer. The energy distribution of the γ-quanta which reaches the detector from the scatterer of thickness d_a , is obtained from (2.62) multiplied by the probability of the radiation leaving the scatterer at an angle γ_2 (Fig. 2.9), and integrated over x from 0 to d_a:

$$J_r(E',S) = \frac{D\,\sigma_0 f f'^2 n_a \Gamma\, \Gamma_a^2\, W(\theta)}{8\pi\, \sin\gamma_1}$$

$$\frac{F_r'}{[(E'-E_s-S)^2+\Gamma^2/4]\,[(E'-E_a)^2+\Gamma_a^2/4]}\,, \qquad (2.63)$$

where

$$F_r' = \frac{1-\exp[-\mu_a(E')d_a\,(\csc\gamma_1+\csc\gamma_2)]}{\mu_a(E')(\csc\gamma_1+\csc\gamma_2)}\,, \qquad (2.64)$$

$$D = d\omega\, d\omega'/(1+\alpha)\,. \qquad (2.65)$$

dω' is the solid angle within which the γ-quanta emitted by the scatterer reach the detector. It is to be noted that the factor D causes the substantial drop in the count rate of the γ-quanta in scattering experiments as compared to those performed in transmission mode. The shape of the energy distribution of the scattered γ-quanta substantially depends on the factor F_r' determined by the experimental geometry.
The calculated distribution for bulk scatterers when all backscattered radiation is detected are presented in Fig. 2.14.

The isomer shift δ and the ratio of linear coefficients for resonant and nonresonant interactions $x = \mu_r/\mu_a$ are the tabulated parameters. The value of μ_r in this case is determined by the enrichment of the resonant isotope. Energies are given in units of $\Gamma_{nat}/2$. A comparison of the dependences shown in Figs. 2.10a and 2.14.2 shows that the interaction of γ-radiation with matter must be taken into account when a real sample, as opposed to the hypothetical case of a single atom scatterer, is considered.

A scatterer can be called thin if the following relation holds

$$t_s = (t_a + t_a^e)\,\mathrm{csc}\gamma_1 + b\,\mathrm{csc}\gamma_2 << 1 . \qquad (2.66)$$

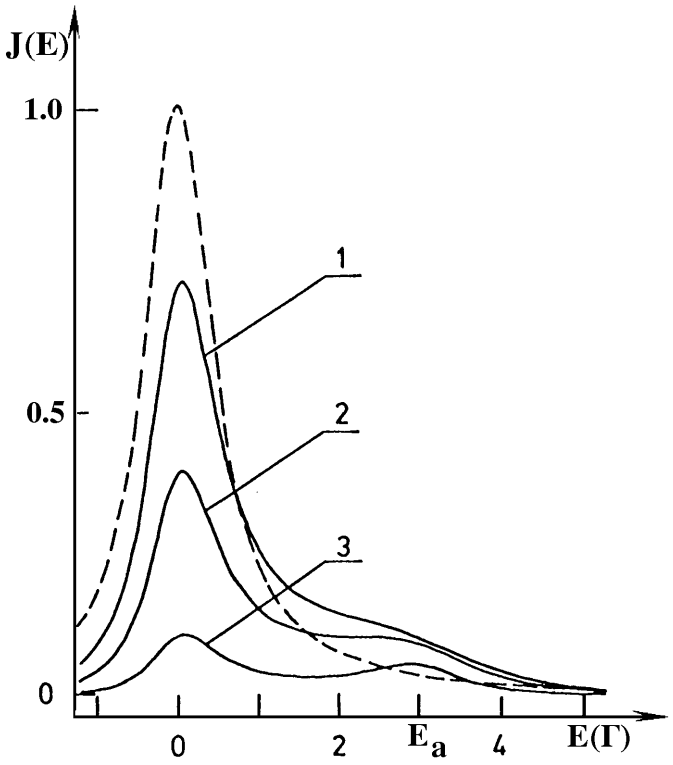

Fig.2.14 Energy distribution of γ-quanta scattered by a bulk sample of non-magnetic iron at different ^{57}Fe abundances. The dashed curve is calculated for x = 128, curve 1 - for x = 8, curve 2 - for x = 4, curve 3 - for x = 1. The zero energy corresponds to the centre of incident radiation spectrum. For convenience the intensities of curves 1 - 3 are enlarged by a factor of 3.

In Mössbauer scattering spectroscopy the effective Mössbauer sample thickness t_a (see (2.8) and (2.23)) used in

transmission spectroscopy together with two more analogous parameters: $t_a^e = \mu_a d_a$; and $b = \nu d_a$, where ν is the linear absorption coefficient for the detected radiation, must also be considered.
The spectrum line shape from thin scatterer (2.64) can be described by the following expression:

$$I_r(S) = \frac{D t_a f f'^2 \Gamma \Gamma_a^2}{8\pi \sin\gamma_1} \int_{-\infty}^{\infty} \frac{W(\theta)\, dE'}{[(E' - E_s - S)^2 + \Gamma^2/4][(E' - E_a)^2 + \Gamma_a^2/4]} . \tag{2.67}$$

Since in this case the lines in the source and the scatterer are Lorentzian, the integral in (2.67) has the value:

$$\int_{-\infty}^{\infty} \frac{dE'}{[(E' - E_s - S)^2 + \Gamma^2/4]\,[(E' - E_a)^2 + \Gamma_a^2/4]} = \frac{8\pi}{\Gamma \Gamma_a (\Gamma + \Gamma_a)} \frac{1}{1 + \left[\frac{2(S - \delta)}{\Gamma + \Gamma_a}\right]^2} . \tag{2.68}$$

If the scatterer is thin, the contribution of the recoillessly scattered γ-quanta into the Mössbauer spectrum is

$$I_r(S) = \frac{D\, t_a f f' W(\theta)}{\sin\gamma_1} \frac{\Gamma_a}{\Gamma + \Gamma_a} \frac{1}{1 + \left[\frac{2(S - \delta)}{\Gamma + \Gamma_a}\right]^2} . \tag{2.69}$$

If the finite thickness of the scatterer is taken into account, the expression for the line shape becomes much more complicated. However, the expression for $I_r(S)$ can be written in the form:

$$I_r(S) = D\, t_a f f' W(\theta) \frac{F_r(2S/\Gamma_a, \beta_r, Q, \Gamma/\Gamma_a)}{1 + \sin\gamma_1 \csc\gamma_2} , \tag{2.70}$$

$$\beta_r^2 = 1 + t_a/\mu_a \quad ; \quad Q = \mu_a d_a (\csc\gamma_1 + \csc\gamma_2) .$$

If the detector registers only nonrecoillessly scattered γ-quanta the beam of γ-quanta $I_{rn}(S)$ can be described by an expression analogous to (2.69) with the exception that f' must be replaced by (1 - f'). These quanta cannot be resonantly absorbed. For the thin absorber the intensities ratio is:

$$I_r(S)/I_{rn}(S) = f'/(1 - f') \ . \qquad (2.71)$$

To obtain $I_{rn}(S)$ which is the contribution of the resonantly scattered nonrecoilless γ-quanta in the total spectrum, it is necessary to make the following substitutions: (1 - f') for f', $F_{rn}(S)$ for $F_r(S)$ and $\beta_{rn}^2 = 1 + t_a/\mu_a(1 + \sin\gamma_1 \csc\gamma_2)$ for β_2^2. The functions $F_r(S)$ and $F_{rn}(S)$ have been calculated for various absorbers and thicknesses and are tabulated elsewhere [2.29]. The tables and plots for $F_{rn}(S)$ can be used for any radiation where the attenuation in the scattering material follows the exponential law. This means that the formalism may also be used when scattered X-rays are detected.

It is now necessary to consider the situation when hyperfine interactions are present, the excited level splitting is such that the distance between the sublevels is much greater than Γ, and the interference effects on scattering from different sublevels are neglected. The resonant scattering occurs at energies $E_{ij} = E_j^e - E_i^g$ which are allowed by the selection rules (see Fig.1.3). The distance between the two ground-state sublevels is denoted by $\Delta_{ii'} = E_i^g - E_{i'}^g$.

It is now possible to consider various contributions to the total spectrum recorded for the sample of α-iron and study the effects of the thickness of the scatterer and of the resonant isotope abundance on the line shape of the experimental spectra, the relative line intensities, and the effects on these of saturation phenomena. The most thorough methodology studies have been carried out by BALKO and HOY [2.41,43] and BARA et al [2.44,45]. The linear resonant scattering coefficient in the presence of hyperfine splitting is

$$\mu_r(E) = \frac{\Gamma_a^2 \, \sigma_0 f' n_a}{4} \sum_{i,j} \frac{W_{ij}(\theta_1, \varphi_1)}{(E - E_{ij})^2 + \Gamma_a^2/4} \ , \qquad (2.72)$$

where θ_1 and φ_1 are the polar and azimuthal angles of γ-rays incident upon the scatterer. The directional correlation function $W_{ij}(\theta_1, \varphi_1)$ for the transition of energy E_{ij} is determined by the corresponding $F_L^M(\theta)$ angular functions. The energy distribution of resonantly scattered recoilless γ-quanta

is determined as before (2.59). However, there is in this situation no unique relation between the energies of the incident and scattered γ-quanta. The scattered quantum may have the energy E' = E of the incident quantum, as well as the energy E' = E - $\Delta_{ii'}$. If θ_2, φ_2 are the polar and azimuthal angles for the scattered γ-rays, the differential resonant scattering cross section when the Lorentzian distribution of the incident radiation is taken into account can be written as

$$\frac{d^3\sigma}{dE\, dE' d\omega} = \frac{\sigma_0 f'^2 \Gamma\, \Gamma_a^2}{8\pi(1+\alpha)} \sum_{i,j,i'} \frac{W_{ij}(\theta_1\varphi_1)\, W_{ji'}(\theta_2,\varphi_2)}{[(E - E' + \Delta_{ii'})^2 + \Gamma^2/4][(E' - E_{ij} - \Delta_{ii'})^2 + \Gamma_a/4]} . \quad (2.73)$$

Let us assume that the correlation functions $W_{ij}(\theta,\varphi)$ are axially symmetric and normalized. The summation in (2.73) is over all the transitions allowed by the selection rules. If the allowed excitation of a sublevel takes place with energy E_j^e , corresponding to the transition $E_i^g \rightarrow E_j^e$ (see, for example transition 3 in Fig.1.3), the decay of the level is possible via the $E_j^e \rightarrow E_i^g$ and $E_j^e \rightarrow E_{i'}^g$ transitions (solid arrows in Fig.1.3). Thus, for scatterers with hyperfine split levels, the energies E of incident- and E' of scattered - γ -quanta may be different. If the source radiation has Lorentzian line shape and the factor f is assumed to be anisotropic (2.59), integration over E gives expression in the form [2.41] :

$$\frac{dJ_r(E',S,x)}{dx / \sin\gamma_1} = \frac{\sigma_0 n_a f f'^2 \Gamma\, \Gamma_a^2}{8\pi(1+\alpha)} \sum_{i,j,i'} \frac{W_{iji'}(\theta)\, e^{-\mu_a (E' - \Delta_{ii'}) \csc\gamma_1 x}\, d\omega}{[(E' - \Delta_{ii'} - E_s - S)^2 + \Gamma^2/4][(E' - E_{ij} - \Delta_{ii'})^2 + \Gamma_a^2/4]} , \quad (2.74)$$

where θ - is the angle between vectors $\underline{k}_0$ and $\underline{k}_f$. If splitting of the levels is such that interference of Mössbauer scattering from different sublevels may be neglected (see Sec. 2.3), the energy distribution of γ-quanta from a scatterer with thickness d_a is obtained by integration of (2.74) over x from 0 to d_a :

$$J_r(E',S) = \frac{D\, a_r \sigma_0 n_a f f'^2 \Gamma\, \Gamma_a^2}{8\pi} \sum_{i,j,i'} \frac{W_{iji'}(\theta)\, F_r'}{[(E' - \Delta_{ii'} - E_s - S)^2 + \Gamma^2/4][(E' - E_{ij} - \Delta_{ii'})^2 + \Gamma_a^2/4]}, \quad (2.75)$$

where the function F_r' is determined by an expression analogous to (2.64)

$$F_r' = \frac{1 - \exp\left\{-d_a[\mu_a(E' - \Delta_{ii'})\ \mathrm{csc}\gamma_1 + \mu_a(E')\ \mathrm{csc}\gamma_2]\right\}}{\mu_a(E' - \Delta_{ii'})\ \mathrm{csc}\gamma_1 + \mu_a(E')\ \mathrm{csc}\gamma_2}, \quad (2.76)$$

where a_r is a constant determined by the particular experimental set-up [2.41].

The Mössbauer spectrum of the resonantly scattered recoilless γ-quanta is given by

$$I_r(S) = \int_{-\infty}^{+\infty} J_r(E',S)\, dE' \quad (2.77)$$

The Mössbauer spectrum $I_{rn}(S)$ due to nonrecoillessly scattered γ-quanta may be obtained by replacing f'^2 by $f'(1 - f')$ and the function F_r' in (2.77) by the function F'_{rn} :

$$F'_{rn} = \frac{1 - \exp\left\{-d_a[\mu_a(E' - \Delta_{ii'})\ \mathrm{csc}\gamma_1 + \mu_a\ \mathrm{csc}\gamma_2]\right\}}{\mu_a(E' - \Delta_{ii'})\ \mathrm{csc}\gamma_1 + \mu_a\ \mathrm{csc}\gamma_2}. \quad (2.78)$$

It is important to note that Rayleigh scattering of the resonant radiation also contributes to the Mössbauer spectrum. The contributions should be distinguished - the elastic Rayleigh scattering of Mössbauer quanta $I_R(S)$ and the inelastic Rayleigh scattering $I_{Rn}(S)$ (see Table 2.4):

$$I_R(S) = \frac{a_R f f_R n' \Gamma\, d\omega\, d\omega'\, W(\theta)}{2\pi(1 + \sin\gamma_1\ \mathrm{csc}\gamma_2)}$$

$$\int_{-\infty}^{\infty} \frac{1 - \exp\left[-\mu_a(E')\, d_a\, (\csc\gamma_1 + \csc\gamma_2)\right]}{\left[(E' - E_s - S)^2 + \Gamma^2/4\right] \mu_a(E')}\, dE' , \qquad (2.79)$$

$$I_{Rn}(S) = \frac{a_R f (1 - f_R)\, n'\, \Gamma\, d\omega\, d\omega' W(\theta)}{2\pi \sin\gamma_1}$$

$$\int_{-\infty}^{\infty} \frac{1 - \exp\left\{-\left[\mu_a(E')\csc\gamma_1 + \mu_a \csc\gamma_2\right] d_a\right\}}{\left[(E' - E_s - S)^2 + \Gamma^2/4\right]\left[\mu_a(E')\csc\gamma_1 + \mu_a \csc\gamma_2\right]}\, dE' , \qquad (2.80)$$

where n' is the number of scattering atoms per unit volume.
Expressions (2.79) and (2.80) were initially used in [2.41] which considered scattering at 90° when $f_R = f'^2$ and the value of the angular term W(θ) was included in the constant a_R which is determined by the Rayleigh scattering cross section and the experimental set-up.
It is convenient to represent the experimental Mössbauer spectrum as the result of the combined action of four processes. If the fraction f is considered of γ -quanta recoillessly emitted from the source, then the total intensity of Mössbauer scattering at a velocity v may be written [2.41] in the form:

$$I(S) = I_r(S) + I_{rn}(S) + I_R(S) + I_{Rn}(S) . \qquad (2.81)$$

The contributions of the individual processes will be analysed in more details in Chapter 4. In backscattering geometry it is necessary to simply integrate over x. The spectra to be expected from (2.81) may be considered by examining an iron powder enriched in ^{57}Fe (a = 91 %) with parameters t_a= 153, f' = 0,7, μ_a = 205 cm^{-1}, and subjected to the calculations described in [2.41]. Difficulties in computation are at the last stage when it is not possible to integrate explicitly (2.75) over E' . The calculations may be substantially simplified by assuming that the radiation which is incident on the scatterer is monochromatic, i.e. Γ = 0. The results are presented in Fig.2.15 and 10^{-3} of the incident radiation intensity is taken as a unit of the scattered radiation intensity.
A characteristic feature of the spectra recorded from elastic resonant scattering as compared with spectra recorded in transmission experiments is the unusual effect of the

scatterer thickness on the line amplitudes. The amplitudes of all the lines approach different limiting values with that of the second line becoming the largest. The reason concerns the velocity v_2 which corresponds to the centre of the second spectral line. At this velocity the scattered radiation $J_r(E', v_2)$ consists of two components contributing to the intensities of the second and fourth lines of the spectra (Fig.1.3). The second component of the scattered radiation is less resonantly scattered than the first component (see Table 2.3). A nonresonant detector would register both components with equal probability. Hence, if attenuation of the scattered beam on the way to the detector is not taken into account the radiation penetration appears to increase and the amplitude of the second line increases as compared to scattering from a single atom. The opposite is true if scattering is at a velocity corresponding to the forth line and penetration of the elastically scattered radiation $J_r(E', v_4)$ appears to decrease in comparison with transmission experiments.

Nonrecoillessly scattered γ-quanta are not resonantly scattered on the way to the detector, and the amplitudes of all the lines of the spectrum $I_{rn}(S)$ are approximately equal.

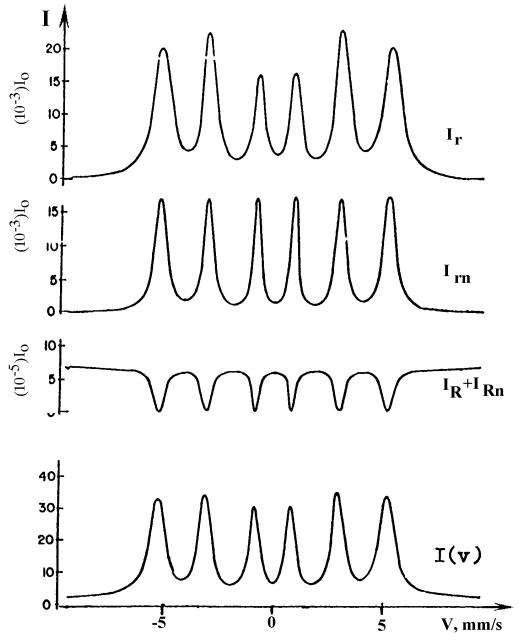

Fig.2.15 Calculated Mössbauer scattering spectrum I(v) and separate contributions to it [2.41].

At resonance velocities the count rate of γ-quanta scattered by electrons is at a minimum. This occurs because the Rayleigh scattering cross section is independent of energy in the energy region of interest: $E_0 \pm 1000$ Ã . The incident γ-quanta passing through the scatterer are strongly attenuated at resonance energies, and the number of γ-quanta capable of Rayleigh scattering on resonance is therefore considerably less than at non-resonant conditions.

Although, we are considering here a thick scatterer enriched in ^{57}Fe, the total intensity of the scattered quanta even for such an ideal case will not exceed several percent of the incident intensity. For nonenriched scatterers the relative contribution of Rayleigh scattering into the total spectrum will be appreciably more than in the case being considered here.

The calculated spectra for thick scatterers of natural iron which correspond to the scattering of monochromatic radiation show neither significant line broadening nor saturation effects. However just the opposite is true for the enriched samples. This can be illustrated by considering the same scatterer but with a = 90 % ^{57}Fe. As the linear coefficient μ_a increases and at

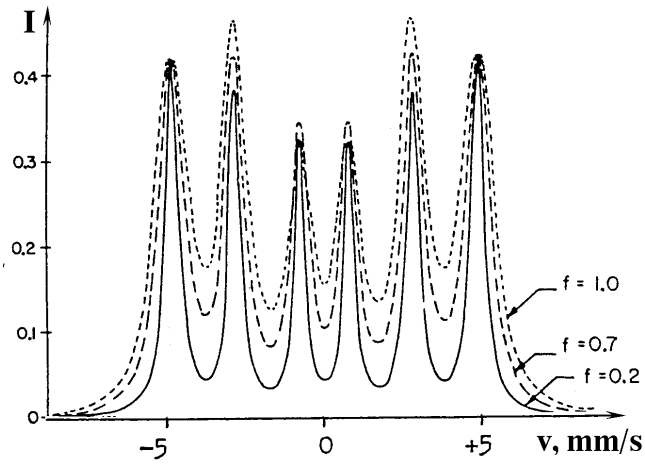

Fig.2.16 Calculated effect of the factor f' on the line shape of scattering Mössbauer spectra. The absorber is iron powder (a = 91 %; μ_a = 200 cm^{-1}; t_a = 175). The spectra are normalized such that the intensities of the first lines are the same [2.41].

constant values of f' and t_a the lines of the Mössbauer spectrum become narrower because the contribution from deeper layers of the sample is less. As the f' factor increases and at constant values of μ_a and t_a the lines are significantly broader (Fig. 2.16) since the situation is equivalent to a higher enrichment of the resonant isotope in the scatterer.

Any attempt to observe the Mössbauer effect in scattering geometry, using only the principles of transmission experiments, would usually produce unsatisfactory results. Even with a scatterer of α-^{57}Fe (see Fig. 2.9) the magnitude of the effect would be in the order of 10 %. A successful experiment requires the proper collimation of the incident and scattered beams and correct distances between the source, the scatterer and the detector. Experience in Mössbauer scattering spectroscopy shows that the optimal geometry is realized in an experimental set-up where the removal of the sample under investigation results in only the γ-radiation caused by single scattering cannot reach the detector. In such a geometry the observed effect in α-^{57}Fe foils is between 150 % and 250 % .

The γ-spectra resulting from the scattering of radiation from a ^{57}Co (Cr) source by a 9 μm α-^{57}Fe foil are shown in Fig. 2.17. There are no filters between the source and the scatterer or between the scatterer and the detector. The solid circles show the amplitude spectrum obtained at a velocity near v_1. Open circles depict the spectrum at v = 0.

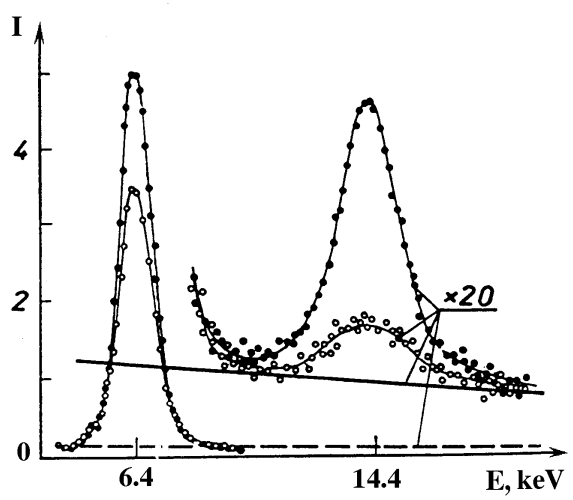

Fig. 2.17 Pulse-height spectra of the ^{57}Co radiation scattered from α-Fe.

The background measured in the absence of the scatterer is given by the solid line. The background detected in the absence of the source is represented by the dashed line. All the lines correspond to the same measuring time and are characteristics of the experimental conditions. The observed effect for the first line of the sextet is about 250 %.

By decreasing the diameter of the collimator and increasing the distance it is possible to exclude the γ-quanta resulting from multiple scattering. This gives an increase in the observed effect but with a decrease in intensity. Examples of this technique are given elsewhere [2.44, 45] where, using a geometry similar to that shown in Fig. 2.9 and with proper collimation, the dependence of the magnitude of the effect on the thickness of ^{57}Fe enriched and nonenriched iron and haematite scatterers have been studied.

Three Mössbauer spectra were recorded simultaneously using scintillation counters. These were the transmission spectrum and both γ- and X-rays scattering spectra. The authors succeeded in substantially lowering the background to obtain a large $\varepsilon(0)$ value.

The dependence of the effect $\varepsilon(0)$ and the intensities on the thickness of a haematite scatterer are shown in Fig. 2.18 [2.45]

$$\varepsilon(0) = [I(0) - I(\infty)]/ I(\infty) . \qquad (2.82)$$

It can be seen that in Mössbauer scattering spectroscopy the maximum effect is observed for the thinnest sample. The largest effect can be observed when the resolution of the detector is high and when it is properly shielded from the hard radiation of the source and from the quanta scattered from surroundings such as the walls of the collimator.

The γ-quanta emitted nonrecoillessly from the source also contribute to the total intensity as a result of Rayleigh scattering and the Compton effect. The fraction of these quanta is (1 - f) and the contribution I_{R+C} is independent of the Doppler energy shift. Therefore, in [2.45] an expression is given for I(S) which contains five terms:

$$I(S) = I_r(S) + I_{rn}(S) + I_R(S) + I_{Rn+C}(S) + I_{R+C} . \qquad (2.83)$$

In the authors' opinion (2.83) is more adequate than (2.81), since it more thoroughly accounts for the interaction of the scattered radiation with the sample. Resonant scattering has different effects on the first four contributions defined in (2.83) to the total Mössbauer spectrum. Thus, $I_r(S)$ depends on resonant scattering when radiation passes into the sample as well as on its way back to the detector. It could be important for selective excitation when the resonant interaction cross sections for the incident and scattered γ-quanta may not be the same.

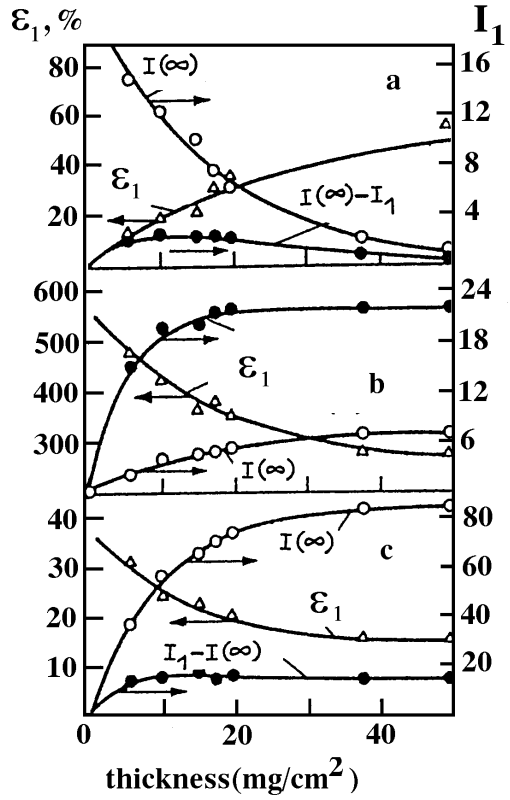

Fig. 2.18 Dependences of the effect value ε_1 and radiation intensities on the sample thickness for the Mössbauer spectrum of haematite (a = 80 %) [2.45]. a - transmission; b and c - scattering (b - γ-rays, c -X-rays).

The terms in (2.83) have their own angular dependences and, in addition, interference is possible between Mössbauer and Rayleigh scattering. However, on considering the angular distribution for I(S), all the interference effects in experiments of interest are usually neglected. There are two reasons for this. First, the contribution of interference to the total intensity is usually small. Second, the requirement to obtain a sufficient count rate leads to the use of large solid angles causing the interference effects to "smear out". It must also be remembered that there is no interference if the energy of the incident γ-quanta corresponds exactly to a resonant absorption peak.

The calculated [2.45] $\varepsilon(v_1)$ values are given in Fig. 2.19 for monochromatic source γ-radiation in transmission and scattering experiments as a function of the thickness of an iron sample for a = 2 % and 100 %, and for a series of hypothetical values of μ_a. The results show good agreement between the calculated results and the experimental data of Fig.2.18.

If relaxation processes or hyperfine interactions occur in the scatterer the interpretation of conventional scattering (or transmission) experiments is often complicated and the results are ambiguous. If the interpretation is possible the information on $\mu_a(E)$ ($\sigma_a(E)$) is usually obtained. The information on $\mu_a(E)$ alone does not help in detailed studies of hyperfine interactions in the samples mentioned above. Of much more help is any direct information on the differential cross sections (see e.g., (2.73) and (2.75)) which are a function of the incident and scattered γ-quanta energy. The incident γ-quanta energy should be fixed and the energy spectrum J'(E', v_i) observed to show directly the energy change of γ-quanta on scattering. If there is no phonon spectrum excitation:

$$J'(E',v_i) = J_r(E',v_i) + J_R(E',v_i) \; . \qquad (2.84)$$

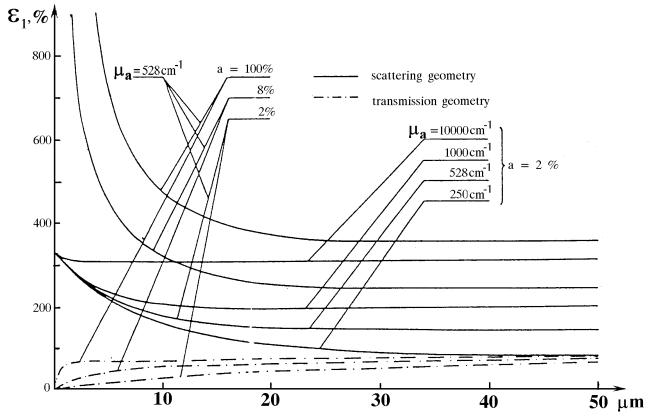

Fig.2.19 Dependence of the effect value ε_1 of the Mössbauer spectrum of iron on the sample thickness d in scattering experiments (solid lines) and in transmission experiments (dashed lines). For samples of natural abundance, hypothetical cases of different μ_a have been considered.

The scattering angle $\theta = 90°$ should be taken for the minimum interference contribution. For a thin scatterer $J_R(E', v_i)$ is always Lorentzian (see Fig. 2.10c). The $J_r(E',v_i)$ distribution gives the necessary information and for a thin sample may be written as

$$I(v,v_i) = \int_{-\infty}^{+\infty} J'(E', v_i)[1-\mu_a'(E',v)\,d]\,dE' \,, \qquad (2.85)$$

where $\mu_a'(E',v)$ is the total linear scattering coefficient in the "analyzer" moving at a velocity v, and d is the "analyzer's" thickness.

It is desirable that the $J'(E', v_i)$ distribution should not be different from the $J_r(E', v_i)$ distribution. For this purpose a constant velocity v_i is chosen so that the incident radiation is on resonance with one of the scatterer's lines. Rayleigh scattering contributes only to the amplitude of the elastic resonant scattering, does not change the line shape, and cannot result in misleading information.

To obtain the $I(v, v_i)$ dependence a γ-ray detector is needed with an energy resolution of approximately $\tilde{A}_{nat}$. For this purpose a resonant filter is placed in front of a conventional detector. This filter is a "single line" Mössbauer absorber and an enrichment in the resonant isotope is desirable. Driving the filter ("analyzer") in the constant acceleration mode and detecting the outgoing radiation allows the $I(v, v_i)$ spectrum to be produced (see Fig. 2.20). The observed effect is determined now by the two elastic resonant scattering processes (by four f factors). Two synchronized drive system are necessary to observe the two scattering processes. This is known as selective excitation double Mössbauer spectroscopy (SEDMS) [2.46 - 48].

The method is demonstrated by considering the SEDM spectrum recorded at $v_i = v_2$ from a 9 μm thick iron foil with a = 90 % ^{57}Fe (Fig. 2.21), that is for scattering at the energy corresponding to the -1/2 $\rightarrow$ -1/2 transition in the scatterer (Fig. 1.3). The Mössbauer spectrum $I(v,v_i)$ consists of the second and fourth lines of the usual spectrum of α-Fe, i.e. the lines corresponding to the -1/2 $\rightarrow$ -1/2 transition as well as to the -1/2 $\rightarrow$ +1/2 transition. The method has been applied to determine the f' factor for the first time in stainless steel [2.46]. Time-dependent effects have subsequently become the main field for SEDMS research [2.49, 50].

A SEDMS theory for time-independent hyperfine interactions has been given elsewhere [1.4, 2.43] and all the necessary energy distributions and SEDM spectral components have been

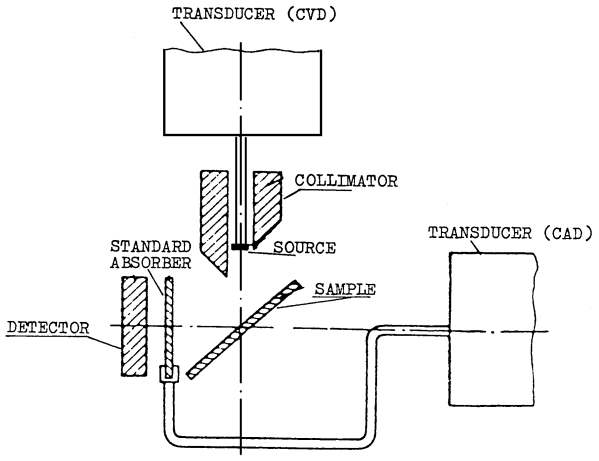

Fig.2.20 A schematic experimental arrangement used for Selective Excitation Double Mössbauer Spectroscopy.

considered. Three processes have been taken into account: resonant- and Rayleigh-scattering, and γ-rays absorption in the scatterer due to the photoeffect. The scattering angle has been selected as 90º. It has been shown that in the experimental spectra a line is always observed at an energy that is exactly equal to the energy of the incident γ-quanta. If this energy coincides with a transition energy in the scatterer, one more fairly intensive line may also appear in the spectrum.

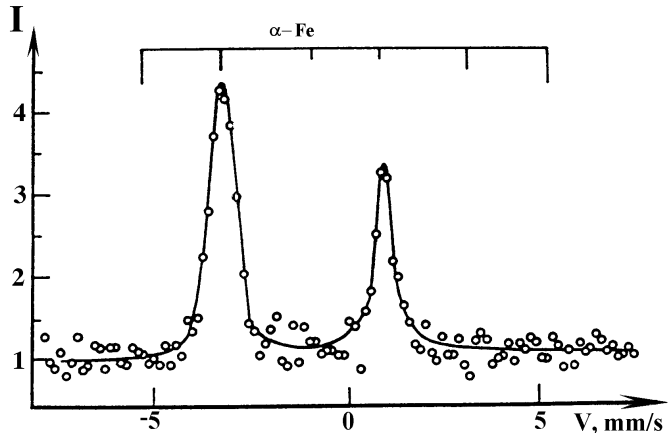

Fig.2.21 SEDM spectrum of α-Fe.

Energies of the incident γ-quanta which are much different from the transition energy in non-enriched scatterers result in the Rayleigh scattering contribution becoming so dominant that in the spectrum a line due to Rayleigh scattering occurs [2.51]. The Rayleigh scattering can be separated out and studied by SEDMS in a different manner. For example, if the velocity v_i is set to excite the -1/2 $\rightarrow$ -1/2 transition then the corresponding line in a SEDM spectrum will contain the Rayleigh scattering contribution although the line -1/2 $\rightarrow$ +1/2 that is observed in the same spectrum will not contain the contribution. By considering all the parameters affecting the line intensity ratio in the Mössbauer effect the Rayleigh scattering cross section can be obtained.

The main advantage of SEDMS is that the method offers a direct means by which the relaxation processes between sublevels of the excited nucleus can be observed. Indeed, the experimental spectrum $I(v,v_i)$ gives direct information on time- dependent hyperfine interactions which determine the nuclear level splitting. The relaxation times in the region of 10^{-7}- 10^{-10} sec are the most convenient to measure. The first studies in this field have been connected with the Morin transition in haematite. In the vicinity of the Morin temperature T_M there is a 90^o change in the direction of spins of iron atoms [2.43]. Below T_M the spins of iron atoms are parallel to the [111] direction, above T_M they are in the (111) plane. Two different Mössbauer spectra correspond to these different orientations (see Fig.2.22). In the transmission spectrum taken at T = 298 K, i.e. above T_M, the sixth line is at v = 8.34 mm/sec (Fig. 2.22.a), and in the spectrum taken at 77 K (below T_M) this line is at v = 9.2 mm/sec (see Fig. 2.22.f). Near T_M (parts of the transmission spectrum, taken at 269.5 K; 265 K; 263.5 K and 261 K are given in Figs. 2.22.b - 2.22.e) the sixth line is significantly broadened and distorted. This may be due to either the existence near T_M of two ionic states with different orientations of the magnetic field direction with respect to the crystallographic axes, or to relaxation phenomena. SEDMS experiments allow these two possibilities to be examined. An experimental spectrum is given in Fig. 2.23 in which the calculated spectrum is shown in the absence of relaxation by the dashed line. The arrow shows the source velocity. The value of the relaxation time in haematite at 263.5 K is $(1.1 \pm 0.2)\cdot 10^{-7}$ sec.

A recent development in SEDMS line shape calculations is the superoperator approach [2.52]. This has made possible the analysis of the effects of various parameters and experimental conditions on the line shape. In studies of a classical paramagnetic tris-(pyrrolydine)dithiocarbamate Fe(III), (TPDC [Fe(III)]), which can be described by any of three possible relaxation models, one has been chosen [2.53]. The authors have shown the relaxation processes to depend on the sample temperature.

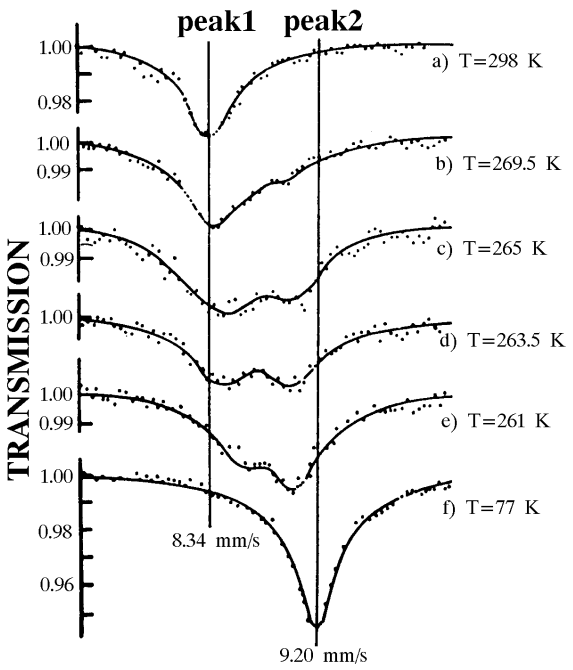

Fig.2.22 Transmission Mössbauer spectra from a thin sample of haematite (a = 90 %) in the vicinity of line VI (see text).

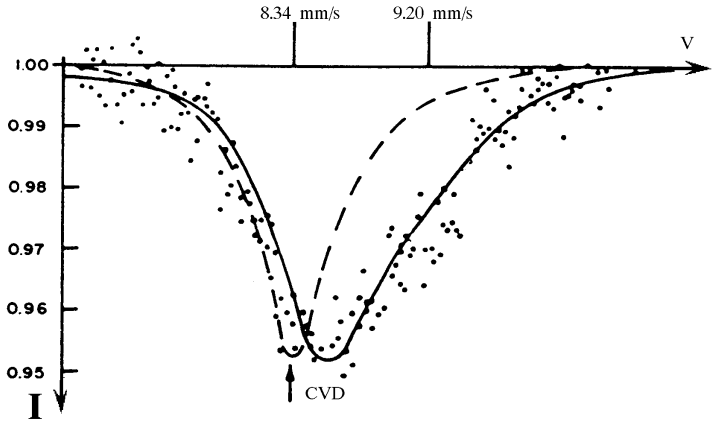

Fig.2.23 SEDM spectrum from a thin haematite sample at 263.5 K. The spectral line shape is given by the solid line calculated for a relaxation time of $1.1 \cdot 10^{-7}$ s.

Thus, at 5.4 K the relaxation is due to transitions between the sublevels of the Kramers doublet corresponding to the ground state. The relaxation rate was found to be in the order of $5 \cdot 10^9$ sec^{-1}. The use of ordinary Mössbauer transmission spectroscopy for similar systems does not permit the selection of the correct relaxation model from several possible ones.

To summarize, it should be noted that SEDMS has some substantial limitations connected with the insufficient strength of Mössbauer sources. The necessity to have two successive resonant interaction processes results in a very low detected intensity. Indeed, the second part of a SEDMS experiment is a transmission experiment with the scatterer being the Mössbauer source. If the levels are split, even for a scatterer enriched in the resonant isotope, the intensity of this source is not more than a percent of the intensity reaching the scatterer from the source. The observed effect in such a transmission experiment with an enriched analyzer is about 10 % (see Fig. 2.23). This means that studies of samples with only natural abundances of Mössbauer isotopes are very time-consuming.

Resonance detectors have been successfully used in Mössbauer emission spectroscopy. Since SEDMS experiments require the energy analysis of the Mössbauer radiation when the scatterer is the source, the use of a resonance detector as the "analyzer" allows a better signal-to-background ratio. A spectrum given in Fig. 2.21 is not typical for SEDMS experiments (cf. Fig. 2.23). It is taken using a resonance detector and the observed effect is several hundred percent. The effect with an ordinary Mössbauer source (without any scatterer) is about 1500 %. Most important in the use of resonance detectors in SEDMS is the low noise level. Thus, the use of a scintillation resonance detector, which is conveniently used in transmission experiments, is not efficient in SEDMS due to the high noise level of the detector. The use of gas-filled resonance detectors allows a shortening of the measuring time by a factor of 9 with the same statistic accuracy. Such resonance detectors can be made very light and the detector itself can be driven. Massive samples of any form may be studied, and SEDMS is a convenient technique in applied fields where the observed spectra are more complicated.

As noted in Sect. 2.3, one of the interference phenomena, the total reflection of ã-rays, may be used for studies of very thin surface layers. It is known that if electromagnetic radiation falls onto a mirror surface characterized by the complex index of refraction $n = 1 - \sigma - i\beta$ at a glancing angle $\gamma_1 \leq \gamma_{cr} \leq \sqrt{2\delta}$ the reflectivity R, i.e. the ratio of the reflected and incident intensities, becomes equal to unity [2.5, 11]. For real media there is always some absorption and the imaginary part of the index of refraction is not zero. However, if the R value rises sharply when γ_1 becomes less than γ_{cr} the situation is described as total external reflection (TER). The coherent amplification of the scattered wave under conditions of TER is analogous to diffraction on scattering from single

crystals. The index of refraction depends on the coherent scattering amplitude $\boldsymbol{F}_{coh}(\underline{k}_0 = \underline{k}_f)$ per scattering centre in the forward direction

$$\delta + i\beta = - \frac{2\pi\, n'}{k_0^2} \mathcal{F}_{coh}(\underline{k}_0 = \underline{k}_f) \ , \qquad (2.86)$$

where n' is the number of scattering centres per unit volume.

Where the scattering of Mössbauer radiation is concerned, $\boldsymbol{F}_{coh}(\underline{k}_0 = \underline{k}_f)$ is a complex scattering amplitude and consists of two contributions: $F_{coh}(\underline{k}_0 = \underline{k}_f)$ and $F_R(\underline{k}_0 = \underline{k}_f)$ [2.54]. As has been noted, near resonance the $F_{coh}(\underline{k}_0 = \underline{k}_f)$ values vary significantly with the incident γ-quanta energy whereas $F_R(\underline{k}_0 = \underline{k}_f)$ remains constant. Thus, the resulting value of $\boldsymbol{F}_{coh}(\underline{k}_0 = \underline{k}_f)$, and hence n and R, depend on γ-quanta energy and velocity v near the resonance. The index of refraction (2.86) depends only on the forward scattering amplitude and hence there is no phase shift between the waves scattered by various atoms and nuclei in the unit cell. Unlike the situation in diffraction, the structure factor of the basis need not be used for the unit cell.

Interference effects and, as a consequence, the dependence of R on the incident γ-quanta energy and the glancing angle γ_1 , have been observed by the Mössbauer effect [2.54-56]. At the same time it has been shown that in the presence of hyperfine splitting and of non-randomly oriented quantization axes in the scatterer, polarization effects should also be taken into consideration. $\boldsymbol{F}_{coh}(\underline{k}_0 = \underline{k}_f)$ must then be replaced by a matrix of forward scattering amplitudes for various polarization components in the incident and scattered radiation. The medium becomes doubly refractive and a single refractive index is insufficient to describe the phenomena observed upon the action of Mössbauer radiation. Moreover, the effect can be sufficiently large to affect the line shape ($\sigma_r(E)$) in Mössbauer transmission spectroscopy.

An experimental set-up is given for studies of TER of Mössbauer quanta in Fig. 2.24 [2.57]. The design of the Mössbauer spectrometer for TER studies ensure: 1) simple and reliable setting and measurement the grazing angle γ_{cr}; 2) convenience in the adjustment of the angular beam divergence; 3) sample replacement without affecting the experimental geometry 4) reproducibility of all source-collimator-sample distances; 5) sample rotation in the range from 0^o to 90^o. The spectrometer consists of the analytical unit and electronic system for control, acquisition and processing of spectrometric data.

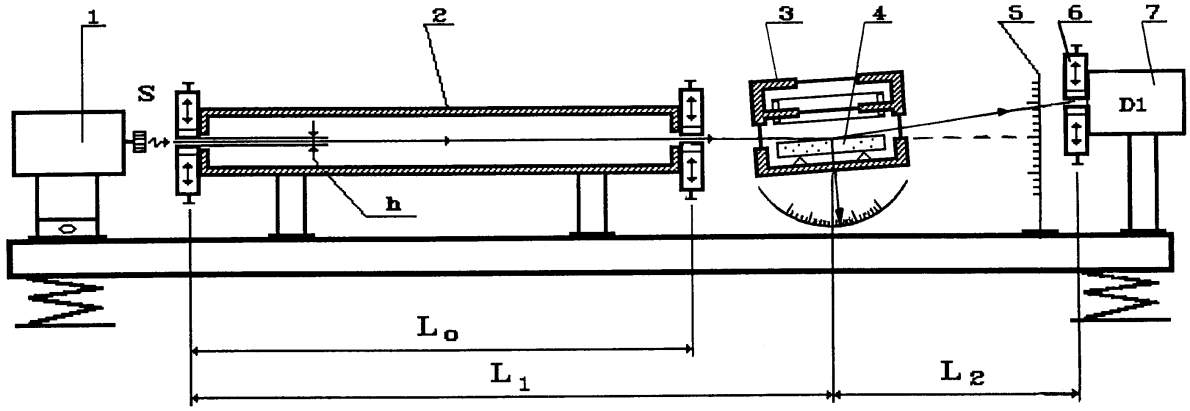

Fig. 2.24 An experimental set-up for studies of total external reflection of Mössbauer quanta. 1 - the Doppler modulator, S - source, 2 - slit collimator, 3 - the dual proportional counter, 4 - sample, 5 - screen, 6 - collimator, 7 - scintillation detector.

The analytical unit of the spectrometer comprises a vibration damping platform suspended on shock-absorbers. Mounted on the platform are guides of the "wedge slide" type which carry the Doppler modulator, shielding screens, collimator to form narrow directed plane-parallel radiation beams, proportional counter and scintillation detector. A narrow plane-parallel γ-rays beam from source S rigidly attached to Doppler modulator is formed by collimator 1 and through the entrance window of the dual detector - 3 falls on the sample 4. The γ-radiation reflected from the sample surface and passed through the exit window of the dual detector and slotted mask 5 is detected by scintillation detector D1.

The geometric dimensions for the analytical part of the spectrometer were optimized based on the following requirements: the divergence value of the collimated γ-rays beam incident on the sample surface must ensure measurements for the angles $\gamma \leq \gamma_{cr}$ and the luminosity should be high enough at the reasonable analytical unit sizes. It is obvious, that near the grazing angle the divergence must be really less, then one half of mrad. As a starting point at the optimization of the geometric dimensions of the spectrometer the active part of the radioactive source were used. Solving the multiparameter optimization problem yielded the following values of basic dimensions and their adjustment intervals for the spectrometer : $<L_o>$ ~ 600 mm, $<L_1>$ ~ 700 mm, $<L_2>$ ~ 400 mm, maximum sizes of collimation slits "h" should be set below 1 mm and adjust with an accuracy better than 0,05 mm.

The critical angle for the metal iron mirror is $\gamma_{cr} = 3.8 \cdot 10^{-3}$ sr [2.51]. On reflection at angles less than γ_{cr} the electromagnetic field intensity falls off rapidly. The penetration depth for the radiation (i.e. the thickness ***L*** of a

layer under study) is taken to be equal to the depth at which the intensity is less by times e. For $\beta = 0$ and $\gamma_1 < \gamma_{cr}$ the asymptotic ***L*** value is

$$\mathcal{L} = \frac{1}{2\sqrt{2}\,\gamma_{cr}\,k_0} . \qquad (2.87)$$

If only the elastic scattering by electrons is considered, ***L*** is evaluated to be 1.3 nm for an iron mirror. In [2.54] the mirror was produced on an optically flat surface of a Pyrex plate by depositing an iron layer (91.2 % ^{57}Fe) 15 nm thick. It was shown that the metal surface, i.e. in the 2 nm thick layer, small amounts of wustite and nonmagnetic iron were present.

Although the analyzed layer is very thin, the technique has not been widely used. The reasons reflect the very low luminosity and difficulties in preparing the special surfaces for analysis. Of no less importance is the fact that interference effects complicate the interpretation of the experimental data. Substantial progress is achieved as shall be explained in Subsec. 3.9, by detecting not the scattered γ-quanta, but the electrons leaving the surface when Mössbauer radiation is incident at an angle which is less than critical. In this situation the intensity of the detected radiation increases and interference effects become less significant.

2.6. Scattering Experiments with Detection of Characteristic X-rays

It is known that Mössbauer transitions are usually highly converted and are followed by the emission of characteristic X- rays and Auger electrons. Typical parameters of characteristic X-rays for iron are given in Table 2.5. It can be seen that the weighted average energy of the K X-rays for Fe is 6.47 keV. The difference between the energies of the X- and γ-rays allows the X-rays to be filtered out of the Mössbauer radiation (see Figs. 2.4 and 2.5).

The detection of the characteristic X-rays instead of γ-rays was used in the first Mössbauer scattering experiments [2.58-60]. Such experiments involving ^{57}Fe were favoured by the fluorescence yield ω and the internal conversion coefficient α being overestimated. In fact the gain in intensity of the detected radiation is not as large as has been previously supposed [2.59] in studies aimed at showing that the scattered γ-radiation was more expedient to measure than the characteristic X-rays. The intensity gain for ^{57}Fe is less than 2.5. Of prime importance for the experimentalist is the quality of the spectrum. The maximum effect at a given intensity is a matter of experience.

Table 2.5
Energies of K-characteristic transitions in iron and their relative intensities.

Transition Type	Transition Energy, eV	Relative Intensity of the Transition
K_{α_1}	6403.9	100
K_{α_2}	6390.9	51.1
K_{β_1}	7058.4	12
K_{β_2}	7058.4	6.1

It is usually believed that in the scattering geometry depicted in Fig.2.9 a larger effect is observed on detection of the scattered γ-quanta, the spectrum quality (see Sect. 4.5) being higher (see Fig. 2.18). This is not generally true. Actually for such a gain it is necessary that the direct radiation does not reach the detector and is properly collimated. The sample must be relatively thin and the resonant isotope abundance must not be low. If any of this conditions is not fulfilled, and also if the parameter D (see (2.65)) is large as is necessary for applied research, the detection of X-rays may be preferable. Experiments involving the detection of different radiations are not competing, but may be considered as supplementing each other. The reason is that the difference in the penetration depth of the Mössbauer radiation and of the characteristic X-rays allows the acquisition of information from layers of different thickness by detecting γ-rays and X-rays in turn. There are exceptions to this however when, for example, the K- X-ray absorption in iron is such that μ_a values for the 14.4 and 6.46 keV rays are close.

Scattering experiments involving the detection of X-rays are easier to interpret because of the absence of resonant self- absorption of the radiation leaving the scatterer. In addition, except for the E1 Mössbauer transition, the detection of the backscattered characteristic X-rays means that interference effects may be neglected since they average out over all directions detected by the detector. This averaging causes the interference terms for the Mössbauer transitions of multipolarity M1 and E2 to cancel each other [2.61-63].

Based on numerical calculations, methods of surface layer analysis have been suggested for different experimental situations [2.64-67]. By assuming that the incident and the scattered radiation are well collimated, the dependence of the areas under the spectra and the intensities of K-X-rays, on the γ_1 and γ_2 angles have been investigated (see Fig. 2.9). The model calculations have been carried out for the two cases: $\gamma_1 = \gamma_2$ and $\gamma_1 + \gamma_2 = 90°$.

It was found that the thickness of the effective surface layer which contributes to the spectrum from iron atoms in any given state j depends on the experimental geometry, the total concentration of iron atoms in the sample and in the state j. The possibility of layer-by-layer analysis has been illustrated by the calculation of areas (A) (Fig. 2.25) in the spectra of a model sample consisting of four different layers which each give a well-resolved spectrum [2.67]. The upper spectrum corresponds to the first layer, the fourth (lowest) layer is the bulk consisting of non-magnetic iron with n_{Fe}= 1.0 (curve 4). The first, second and third layers were 3 μm thick with n_{Fe} = 0.9, 0.8 and 0.7, respectively (curves 1,2,3 in Fig. 2.25). The areas under the spectra are given for the two geometric arrangements in Fig. 2.25a for $\gamma_1 + \gamma_2 = 90°$ and in Fig. 2.25b for $\gamma_1 = \gamma_2$.

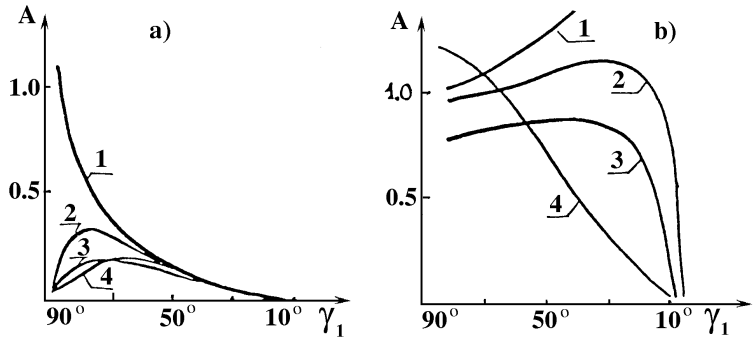

Fig. 2.25 Areas under the partial spectra from three layers (1,2 and 3) successively deposited onto a bulk sample, and the area of the spectrum from the bulk (4). a) $\gamma_1 + \gamma_2 = 90^o$; b) $\gamma_1 = \gamma_2$.

The two dependences show that there may be two ways of layer-by- layer analysis. By the first one, in the geometry $\gamma_1 + \gamma_2 = 90^o$, the succession of the layers and their composition are revealed on decreasing the angle of incidence from 90º to 45º. First, the spectrum from a layer of the minimum thickness is obtained, using the maximum angle of incidence γ_1 , and then by decreasing γ_1 the thickness of the analyzed layer is increased. By the method of successive approximations, adding and subtracting the spectra, it is possible to evaluate the thickness of the layers and their order. If the Mössbauer spectra corresponding to different layers overlap, the problem is too complicated and will be treated in a general form later in Chapter 4.

In the second method the angle of incidence is set equal to the scattering angle. The first spectrum is recorded at a minimum angle γ_1. The successive spectra are taken at larger γ_1 angles. The rest of the procedure is the same as for the first method. If collimation of the incident and scattered radiation is fairly good, it is possible to change the thickness of the analyzed layer from several micrometres to several tens of micrometres simply by changing the angle of the incident radiation. The effect and the line widths depend also on the solid angles $d\omega$ and $d\omega'$ (see Fig. 2.9). It is desirable that $d\omega$ and $d\omega'$ should be less than 5º, since larger radiation divergences diminish the contribution to the Mössbauer spectrum of the sample layers which are nearer to the surface. It should be noted that a better collimation of the radiation beam to increase the depth resolution necessitates longer measurements.

Other sources of the characteristic X-rays may substantially complicate the interpretation of the experimental data. In general the multiple scattering processes should be accounted for. Usually γ-quanta of higher energies are also emitted from the source and the photoeffect due to these quanta may contribute to the detected intensity. In the sample material there may be atoms whose characteristic X-rays are close in energy to the X-rays of interest and hence these are also detected. If the energy is higher, this relatively hard radiation may cause the subsequent emission of experimentally detectable characteristic X-rays. A limitation of the technique is that it is not possible to study a rough surface, for example, the surface of fractures.

The backscattering geometry of Fig. 1.9c makes it possible to work with intensities which are ten times as high as those given in Fig. 2.9. The backscattering geometry is not so flexible but it is simple, efficient, and suitable for any type of radiation. However, to detect γ-quanta a special detector is needed.

The principles of backscattering Mössbauer spectroscopy with detection of X-rays in the 2π solid angle have been given earlier in [2.68] devoted to forward scattering. The technique has also been used in studies of very thin films. The films were placed onto the detector window (Fig. 2.26). The X-rays of the source were filtered off and all X-rays leaving the scatterer were detected. In such experiments the only source of the background is the low photoeffect due to the 14.4 keV γ-quanta.

The scattered radiation may be at any angle θ ($0 < \theta < \pi/2$) with respect to the surface (see Fig. 2.26). The intensity of X- rays scattered as a result of the Mössbauer effect at an angle θ from the layer dx at a depth x is given by:

$$I_x(v,x,\theta) = \frac{C_x}{2} \int_{\infty}^{\infty} \mu_r(E)\, J_M(E,v,x)\, e^{-\nu_x(d_a-x)/\cos\theta} \sin\theta\, dE, \quad (2.88)$$

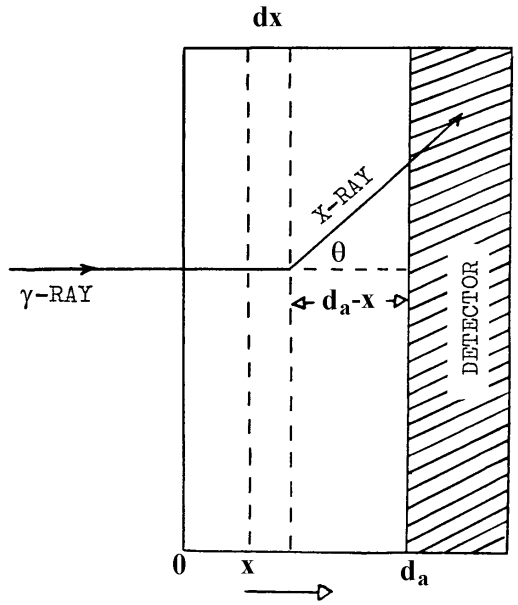

Fig. 2.26 Schematic diagram for studies of thin films in a forward-scattering geometry.

$$C_x = \omega \alpha_K / (1 + \alpha) , \qquad (2.89)$$

where $J_M(E,v,x)$ is given by (2.57) for $\csc\gamma_1 = 1$, ν_x is the total linear absorption coefficient for the X-rays.

The required integration over θ complicates the expression for the lineshape and the evaluation of the area under the spectrum. The area can be evaluated using the approximation method described elsewhere [2.67]. The area under the spectrum determined by (2.88) may be estimated in the following manner. Let the velocity change be linear from $-v_{max}$ to $+v_{max}$ with a period ô. In this case $dt = dv(\tau/2v_{max})$ and integration over v may be replaced by integration over t.

$$A = \frac{C_x f}{\pi \Gamma} \int_0^{\tau} \int_{-\infty}^{\infty} \int_0^{d_a} \int_0^{\pi/2} L(E,v)\, \mu_r(E)\, \exp(-G)\, \sin\theta\, d\theta\, dx\, dE\, dt ,$$

where $G = [\mu_{ph} + \mu_r(E)]x + \nu_x(d_a - x) / \cos\theta$, $\mu_a \approx \mu_{ph}$. The integration over one cycle of the velocity change and also over scattering angles and γ-quanta energies yields the following:

$$A_\tau \simeq \frac{C_x\, f\, \tau\, \mu_r}{8\, v_{max}} \int_0^d \exp[-(\mu_r/2 + \mu_a)x]\, J_0(i\mu_r x/2)\, H(\nu_x(d_a - x))\, dx, \qquad (2.90)$$

where

$$H(s) = \int_0^{\pi/2} e^{-s/\cos\theta} \sin\theta\, d\theta =$$

$$1 + s(\ln s - 0.42) - \sum_{n=2}^{\infty} (-1)^n\, s^n/[(n-1)\, n!] \; .$$

By means of (2.90) and assuming that $\mu_a << \mu_r$, numerical calculations have been carried out [2.68] of areas under Mössbauer spectra and their dependence on the scatterer thickness.
To estimate the possibilities of studying thin films in the forward scattering geometry, the above mentioned dimensionless parameters $t_a = \mu_r d_a$, $t_a^e = \mu_a d_a$, $b = \nu_x d_a$
can be used. The film is thin if the following conditions are fulfilled simultaneously:

$$t_a << 1 \; , \; t_a^e << 1 \; , \; b << 1 \; . \qquad (2.91)$$

The question as to whether transmission geometry or scattering geometry is a more efficient means to study these films can now be approached. The efficiency is the time required to record spectra of the same statistical accuracy. In general, this time depends on both the areas under the spectra and the signal-to-background ratio. For thin films the area may be evaluated by the expression:

$$A \simeq \frac{C_x f t_a}{8\, v_{max}} \left[1 - \frac{t_a^e}{2} - \frac{t_a}{2} \frac{1}{2} - \frac{\nu_x}{\mu_r} \left[\ln\left[\frac{\nu_x}{\mu_r} t_a \right] - 1 \right] \right] . \qquad (2.92)$$

Even for $\nu_x/\mu_r = 2$, the contribution of the last term is small.
The ratio of the area under the spectrum recorded from scattering experiments to that recorded from transmission experiments is $C_x / 2$. In the limiting case of $C_x \rightarrow 1$ the ratio may reach 0.5. For ^{57}Fe it is 0.15. The fact that the area in transmission experiments is larger does not mean that the transmission experiments are more informative.